RESPIRATORY INFORMATION IN ARTERIAL OXYGEN SATURATION MEASUREMENT

Yue-Der Lin
Department of Automatic Control Engineering
Master Program of Biomedical Informatics and Biomedical Engineering
Feng Chia University, 100 Wenhwa Road, Seatwen, Taichung 406, Taiwan

Keywords: Pulse oximeter, Photoplethysmography (PPG), Arterial oxygen saturation (SpO_2), Multi-channel autoregressive (AR) spectral estimation, Coherence analysis.

Abstract: Pulse oximeter has become a standard in intensive and critical care units for the monitoring of oxygen support from respiratory system since 1990's. The multi-wavelength photoplethysmography (PPG) technique is now utilized for the measurement of arterial oxygen saturation by pulse oximeter (SpO_2). This research utilized multi-channel autoregressive (AR) spectral estimation method for the coherence analysis between the respiratory signal and the PPG signal derived from pulse oximeter. Five healthy male subjects participated in this research with signals being measured at different respiratory status. The results demonstrate high coherence between respiration and the PPG signal from pulse oximeter, and the coherence disappears in breath-holding experiments. The results demonstrate that the respiratory status can also be acquired from the measurement of arterial oxygen saturation. This implies the possibility to acquire the physiological parameters other than arterial oxygen saturation form pulse oximeters.

1 INTRODUCTION

Pulse oximetry is a non-invasive method widely used in clinical environments for the analysis of oxygen delivery. Two-wavelength (660 nm and 940 nm) photoplethysmography (PPG) technology is utilized for the measurement of arterial oxygen saturation (SpO_2) in most commercial pulse oximeters (Webster, 1997). In addition to the reading of arterial oxygen saturation, pulse oximeters also provide PPG signal (940-nm wave-length in general) for pulse rate or heart rate monitoring.

PPG signal represents the volumetric changes in blood vessels. Such blood volume change occurs mainly in the arteries and arterioles. The principle of PPG is that the light (mainly red, infrared or green light) traveling through biological tissue (e.g. the fingertip or earlobe) will be absorbed by different absorbing substances, including skin pigmentation, bone, and arterial and venous blood. The arteries contain more blood during systole than during diastole, and their diameter increases due to the increased blood pressure. The detected light reflected from or transmitted through the vessels will thus fluctuate according to the pulsatile blood flow during the circulation. Therefore, the PPG signals are composed of two components, the alternating part of total absorbance due to the pulsatile component of the arterial blood (AC component) and the absorbance due to venous blood, the part of the constant amount of arterial blood, and other non-pulsatile components such as skin pigmentation (DC component) (Hertzman and Spielman, 1937).

As the AC component of PPG signal is synchronous with the heart beat and thus can be identified as a source of heart rate information. In addition, the PPG signal is claimed to contain respiratory-induced intensity variations (RIIV) (Johansson et al., 1999; Nilsson et al., 2000). The so-called RIIV is a kind of modulation arises from the respiratory-induced variations in venous return to the heart. Such variation is primarily caused by the alterations in intrathoracic pressure during respiration. A part of the respiratory-related drift in perfusion also originates from the autonomous control of the peripheral vessels and is also synchronous with respiration. RIIV signal can be extracted from PPG by a bandpass filter (0.13-0.48 Hz). High coherence has been shown to exist

Lin Y. (2010).
RESPIRATORY INFORMATION IN ARTERIAL OXYGEN SATURATION MEASUREMENT.
In *Proceedings of the Third International Conference on Bio-inspired Systems and Signal Processing*, pages 168-173
DOI: 10.5220/0002693501680173

between RIIV and the changes in tidal volume and respiratory rate (Johhansson et al., 1999a and 1999b; Nilsson et al., 2003). As some commercial pulse oximeters also provide PPG signal, these results imply that the pulse oximeters can be a potential tool for the acquisition of arterial oxygen saturation, heart rate and respiration at the same time.

The relationship between RIIV and respiratory signal has been examined extensively in the past decades (Johhansson et al., 1999a and 1999b; Nilsson et al., 2003). However, little research has been done concerning the coherence between the raw PPG signal acquired from pulse oximeter and respiratory signal. As the RIIV may deviate with the varying respiratory rate, the fixed bandpass filter for PPG signal filtration may limit the accuracy of analysis in practical conditions, especially in slow and fast breathing cases. The objective of the present study was to investigate whether such coherence exists between raw PPG signal and respiratory signal. The multi-channel autoregressive (AR) spectral estimation method proposed by Morf et al. (1978), was utilized for the coherence analysis under different breathing rates and the breath-holding state for five healthy male subjects. The two-channel AR-based cross-spectral analysis demonstrated that raw PPG signal and respiration were coherent (magnitude-squared coherence greater than 0.5) at the respiratory frequency in the subjects studied, with changes in respiration leading to changes in PPG. No coherence was found in breath-holding cases for the subjects participated. The results of this research verify that there exists the corresponding respiratory component in spectrum of raw PPG signal. The results may provide another attractive approach to acquire the respiratory information from PPG without the need of filtering. The results also imply the possibility to acquire the physiological parameters other than arterial oxygen saturation form pulse oximeters.

2 METHODS AND MATERIALS

2.1 Subjects and Experiments

Five healthy male subjects (non-smoker and with no prior history of cardiovascular disease) aged between 22 and 24 took part in the experiments after giving the informed consent. All subjects were asked to refrain from caffeine and alcoholic drink at least 4 hours before the experiments. All of the experiments were performed at the same university laboratory with the room temperature being maintained at about 25 degrees centigrade during the night time (from 9 to 11 pm). The subjects were required of having a resting period of at least 5 minutes under relaxation status before the experiment.

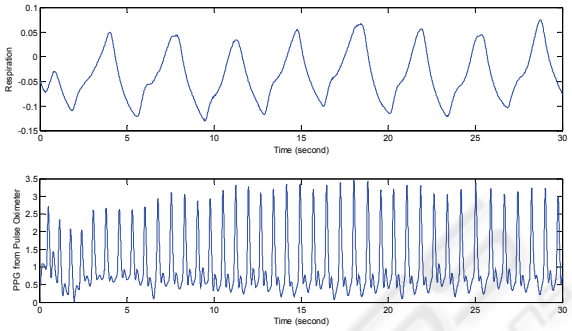

Figure 1: Typical signals acquired. Upper: respiratory signal (natural respiration); lower: PPG signal derived form pulse oximeter.

Each experiment included two stages classified by different respiratory rate (natural respiration and holding the breath in order). Each stage was maintained at least one minute, and the intervals between stages were three minutes. Throughout the experiment, the subjects were seated in a comfortable chair with their right upper arm kept at the height of heart level.

2.2 Signal Measurement

The physiological data acquisition system MP150® (Biopac Inc.) was utilized for signal measurement. Pulse oximetry signal (by pulse oximeter module OXY100C) and respiratory signal (by temperature amplifier module SKT100C with fast response thermistor sensor TSD202A) were collected simultaneously during each experimental stage. The Pulse oximetry probe (TSD123A, with infrared wavelength 910 nm) was attached to the right index finger, whereas the respiratory signal was acquired at the nostril during the measurement. The analysis package Biopac AcqKnowledge® (version 3.9.1) was used for signal management, including the signal quality pre-screening, data storage and retrieval. The signals were verified visually by a well-trained technician. A typical respiratory signal and PPG signal acquired form pulse oximeter are shown in Figure 1. If the signal quality was poor, the signal would be excluded from further analysis and the subject was asked to repeat the experiment once again.

As the dominant components of the processed signals primarily locate around the frequencies below 6 Hz, a sampling frequency of 60 Hz is

enough. However, the ECG (electrocardiogram) measurement is sometime needed in the experiments for timing reference. A sampling frequency of 250 Hz was selected in this research to assure all the signals could be acquired without aliasing. Before the signal analysis, both respiration and PPG signal were down-sampled by a factor of 4.

2.3 Signal Analysis

The source code for multi-channel AR spectral estimation was developed in MATLAB® version 7.3.0 (MathWorks Inc.). The estimation method was originally developed by Morf et al. (1978). It is an expansion of single-channel Levinson recursion algorithm (Levinson, 1947). Two-channel case is introduced as below. The same procedure can be easily expanded to the cases which are more than two channels.

Let $\boldsymbol{x}[n]$ denote the vector of samples from two-channel process at sample index n

$$\boldsymbol{x}[n] = [x_1[n] \;\; x_2[n]]^H , \tag{1}$$

where the superscript ^{H} represent the transpose operation. In this research, $x_1[\cdot]$ and $x_2[\cdot]$ represent the acquired respiratory signal and the PPG signal from pulse oximeter respectively. The two-channel AR(p) model, assumed to be wide-sense stationary, can be represented as

$$\boldsymbol{x}[n] = -\sum_{k=1}^{p} \boldsymbol{A}_p(k)\boldsymbol{x}[n-k] + \boldsymbol{e}_p^f[n] , \tag{2}$$

in which the $\boldsymbol{A_p}(k)$ are the 2×2 AR(p) forward prediction parameter matrices and $\boldsymbol{e}_p^f[n]$ is a 2×1 vector representing the forward linear prediction error or the AR(p) driving noise process. With the property that the driving noise process is uncorrelated with past values of the AR process, the multichannel Yule-Walker normal equations of forward linear prediction version can be derived as

$$\boldsymbol{a}_p\boldsymbol{R}_p = [\boldsymbol{P}_p^f \;\; \boldsymbol{0} \cdots \boldsymbol{0}], \tag{3}$$

with

$$\boldsymbol{a}_p = [\boldsymbol{I} \;\; \boldsymbol{A}_p(1) \cdots \boldsymbol{A}_p(p)] , \tag{4}$$

$$\boldsymbol{R}_p = E\{\boldsymbol{x}_p[n]\boldsymbol{x}_p^H[n]\} , \tag{5}$$

and

$$\boldsymbol{x}_p[n] = [\boldsymbol{x}[n] \;\; \boldsymbol{x}[n-1] \cdots \boldsymbol{x}[n-p]]^H . \tag{6}$$

In the above equations, $\boldsymbol{0}$ are 2×2 null matrices and $\boldsymbol{I}$ denotes a 2×2 identity matrix. The symbol E represents the expectation operator, and $\boldsymbol{P}_p^f = E\{\boldsymbol{e}_p^f[n]\boldsymbol{e}_p^{fH}[n]\}$ is the covariance matrix of the driving noise process for the forward AR(p) process.

The corresponding multichannel Yule-Walker equations for the backward parameter $\boldsymbol{B}_p(\cdot)$ can also be derived in a similar way as

$$\boldsymbol{b}_p\boldsymbol{R}_p = [\boldsymbol{0} \cdots \boldsymbol{0} \;\; \boldsymbol{P}_p^b] , \tag{7}$$

in which

$$\boldsymbol{b}_p = [\boldsymbol{B}_p(p) \cdots \boldsymbol{B}_p(1) \;\; \boldsymbol{I}] . \tag{8}$$

The matrix $\boldsymbol{P}_p^b = E\{\boldsymbol{e}_p^b[n-1]\boldsymbol{e}_p^{bH}[n-1]\}$ is the covariance matrix of the driving noise process for the backward AR(p) process.

The matrix $\boldsymbol{R}_p$ has a Hermitian and a block-Toeplitz structure. On a matrix element-by-element basis, the prediction parameter matrices possess the recursion relationships

$$\boldsymbol{A}_{p+1}(k) = \boldsymbol{A}_p(k) + \boldsymbol{A}_{p+1}(p+1)\boldsymbol{B}_p(p+1-k) \tag{9}$$

$$\boldsymbol{B}_{p+1}(k) = \boldsymbol{B}_p(k) + \boldsymbol{B}_{p+1}(p+1)\boldsymbol{A}_p(p+1-k) \tag{10}$$

for k=1 to p. Define $\boldsymbol{P}_p^{fb} = E\{\boldsymbol{e}_p^f[n]\boldsymbol{e}_p^{bH}[n-1]\}$, i.e. $\boldsymbol{P}_p^{fb}$ is the cross correlation between the forward and backward linear prediction residuals at one unit of delay. Then the normalized partial correlation, a counterpart to the single-channel reflection coefficient in multichannel case, can be derived as

$$\boldsymbol{\Lambda}_{p+1} = \left(\boldsymbol{P}_p^{f\,1/2}\right)^{-1} \boldsymbol{P}_p^{fb} \left(\boldsymbol{P}_p^{b\,1/2}\right)^{-H} , \tag{11}$$

in which the superscript $^{1/2}$ denotes the lower triangular matrix obtained by the Cholesky decomposition of the Hermitian matrix, and the superscript $^{-H}$ represents the matrix Hermitian of its inverse. And then, $\boldsymbol{A}_{p+1}(p+1)$ and $\boldsymbol{B}_{p+1}(p+1)$ can be expressed in terms of $\boldsymbol{\Lambda}_{p+1}$ as

$$\boldsymbol{A}_{p+1}(p+1) = -\left(\boldsymbol{P}_p^{f\,1/2}\right)\boldsymbol{\Lambda}_{p+1}\left(\boldsymbol{P}_p^{b\,1/2}\right)^{-1} \tag{12}$$

and

$$\boldsymbol{B}_{p+1}(p+1) = -\left(\boldsymbol{P}_p^{b\,1/2}\right)\boldsymbol{\Lambda}_{p+1}^H\left(\boldsymbol{P}_p^{f\,1/2}\right)^{-1} \tag{13}$$

respectively. In addition, the order update for the covariance matrix of the driving noise process can also be derived by

$$\boldsymbol{P}_{p+1}^f = [\boldsymbol{I} - \boldsymbol{A}_{p+1}(p+1)\boldsymbol{B}_{p+1}(p+1)]\boldsymbol{P}_p^f \tag{14}$$

and

$$\boldsymbol{P}_{p+1}^b = [\boldsymbol{I} - \boldsymbol{B}_{p+1}(p+1)\boldsymbol{A}_{p+1}(p+1)]\boldsymbol{P}_p^b . \tag{15}$$

Finally, the relationships of the driving noise process between AR(p) and AP(p+1)can be obtained by

$$\boldsymbol{e}_{p+1}^f[n] = \boldsymbol{e}_p^f[n] + \boldsymbol{A}_{p+1}(p+1)\boldsymbol{e}_p^b[n-1] \tag{16}$$

and

$$\boldsymbol{e}_{p+1}^b[n] = \boldsymbol{e}_p^b[n-1] + \boldsymbol{B}_{p+1}(p+1)\boldsymbol{e}_p^f[n] . \tag{17}$$

The above procedure is summarized in Table 1. It is assumed that there are N samples in each channel and the order of two-channel AR process is P.

For two-channel AR spectral estimation, define the complex exponential vector $\boldsymbol{E}_P(f)$ of P+1 block elements as

$$\boldsymbol{E}_P(f) = [\boldsymbol{I} \;\; e^{j2\pi \cdot f \cdot T}\boldsymbol{I} \cdots e^{j2\pi \cdot f \cdot P \cdot T}\boldsymbol{I}], \tag{18}$$

in which T is the evenly sampled interval (sec) of the signals $\boldsymbol{x}[\cdot]$. After the computation of the related coefficients, the power spectrum density (PSD) can be calculated by

$$\boldsymbol{P}_{AR}(f) = T[\boldsymbol{a}_P \boldsymbol{E}_P^H(f)]^{-1} \boldsymbol{P}_P^f [\boldsymbol{E}_P(f)\boldsymbol{a}_P^H]^{-1} \tag{19}$$

$$= \begin{bmatrix} P_{11}(f) & P_{12}(f) \\ P_{21}(f) & P_{22}(f) \end{bmatrix}, \tag{20}$$

where $\boldsymbol{a}_P$ is defined in (4).

The magnitude squared coherence (MSC)

$$C(f) = \frac{|P_{21}(f)|^2}{P_{11}(f)P_{22}(f)} \tag{21}$$

and the coherence phase

$$\theta(f) = \tan^{-1} \frac{\mathrm{Im}\{P_{21}(f)\}}{\mathrm{Re}\{P_{21}(f)\}} \tag{22}$$

versus frequency f are utilized for the coherence analysis between respiration and the PPG signal acquired from pulse oximeter in this research. From equation (20), $P_{11}(f)$ and $P_{22}(f)$ versus f are the PSD of respiration and PPG signal respectively.

3 RESULTS AND DISCUSSION

The coherence between the respiratory signal and the PPG signal acquired from pulse oximeter at different breathing status for five subjects was analyzed to evaluate their relationships in frequency domain. Though only the results for one subject are demonstrated in this paper, similar results are derived for all subjects.

Figure 2 shows the coherence analysis results for one subject in the condition of natural frequency. As seen in Figure 2(a), there exists a peak of MSC greater than 0.5 near 0.2 Hz (the respiratory frequency, see Figure 2(b)). Also, the coherence phase is smaller than zero (see Figure 2(a)), which imply that the changes due to respiration in PPG lags the respiratory signal. It also can be appreciated that there is one corresponding component near the respiratory frequency in the spectrum of PPG signal, as depicted in the lower trace of Figure 2(b). This component is relatively smaller in magnitude compared with the dominant peaks which relate directly to the heart beats.

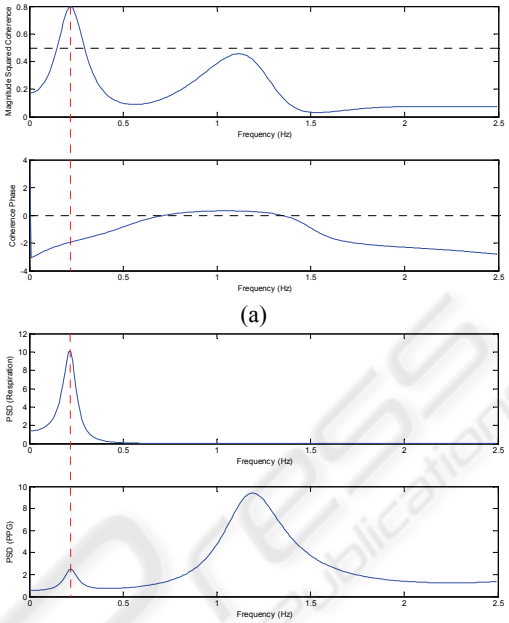

(a)

(b)

Figure 2: Coherence analysis results for the case of natural respiration: (a) MSC (upper) and coherence phase (lower), (b) PSD of respiratory signal (upper) and PPG signal (lower).

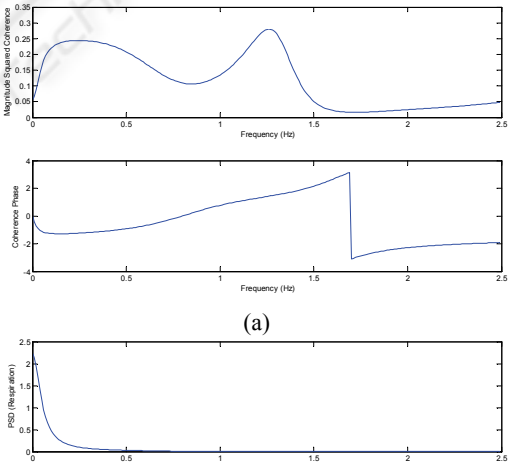

(a)

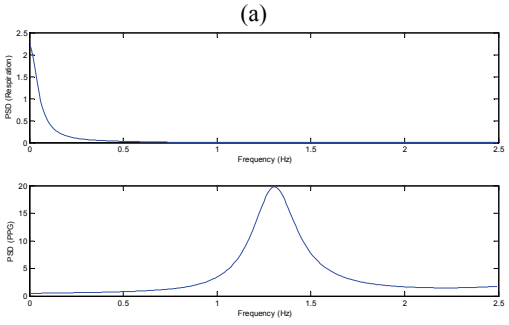

(b)

Figure 3: Coherence analysis results at the breath-holding condition: (a) MSC (upper) and coherence phase (lower), (b) PSD of respiratory signal (upper) and PPG signal (lower).

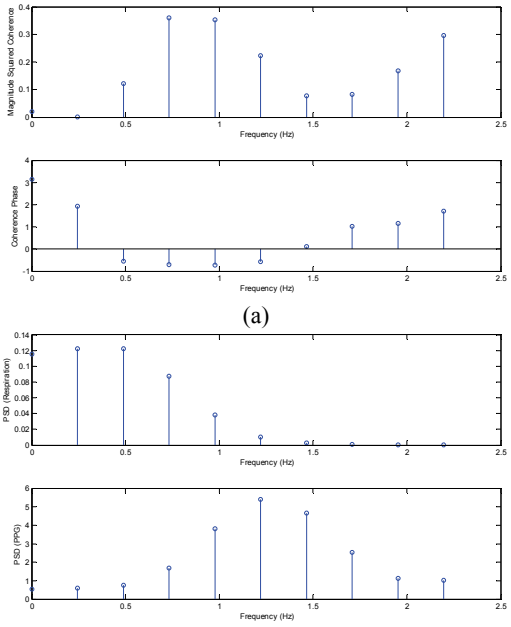

Figure 4: The results by FFT-based cross-spectrum analysis for the case of natural respiration: (a) MSC (upper) and coherence phase (lower), (b) PSD of respiratory signal (upper) and PPG signal (lower).

The results in the breath-holding condition for the same subject are demonstrated in Figure 3 with the same order arranged in Figure 2. As all of the MSC values are less than 0.5 (see Figure 3(a)), it is appreciated that no coherence is found in such case.

The results derived by FFT-based cross-spectrum analysis are demonstrated in Figure 4 (natural respiration case for the same subject). The utilized method is Welch's estimate of periodogram (Welch, 1970) with Hanning window of length 128, 256-point FFT and 64-point overlapping. It can be appreciated that the coherence is not evident as using Fourier-based techniques. One primary reason may arise from the limited frequency resolution of FFT-based techniques.

4 CONCLUSIONS

This study utilized multi-channel AR spectral estimation method to investigate the coherence between the respiratory signal and PPG signal acquired from pulse oximeter under different respiratory status. The Morf's algorithm (Morf et al., 1978) was used for the computation of two-channel AR parameters. The algorithm is summarized in Table 1. The AR-based coherence analysis results

Table 1: Morf's Algorithm.

Let $\boldsymbol{X} = [\boldsymbol{x}[1]\ \boldsymbol{x}[2] \cdots \boldsymbol{x}[n] \cdots \boldsymbol{x}[N]]$

and P = the order of bivariate AR model.

Initialization : $\begin{cases} \boldsymbol{e}_0^f[n] = \boldsymbol{e}_0^b[n] = \boldsymbol{x}[n] \quad for\ n = 1,2,\cdots N \\ \boldsymbol{P}_0^f = \boldsymbol{P}_0^b = \boldsymbol{X}\boldsymbol{X}^H / N \end{cases}$

Computation :

$p = 0$

while $p \le P$

$$\begin{cases} \boldsymbol{P}_p^f = \dfrac{1}{N}\displaystyle\sum_{n=p+2}^{N} \boldsymbol{e}_p^f[n]\boldsymbol{e}_p^{fH}[n] \\ \boldsymbol{P}_p^b = \dfrac{1}{N}\displaystyle\sum_{n=p+2}^{N} \boldsymbol{e}_p^b[n-1]\boldsymbol{e}_p^{bH}[n-1] \\ \boldsymbol{P}_p^{fb} = \dfrac{1}{N}\displaystyle\sum_{n=p+2}^{N} \boldsymbol{e}_p^f[n]\boldsymbol{e}_p^{bH}[n-1] \end{cases}$$

$p = p + 1$

$$\begin{cases} \boldsymbol{A}_{p+1}(p+1) = -\boldsymbol{P}_p^{fb}\left(\boldsymbol{P}_p^b\right)^{-1} \\ \boldsymbol{B}_{p+1}(p+1) = -\left(\boldsymbol{P}_p^{fb}\right)^H\left(\boldsymbol{P}_p^f\right)^{-1} \end{cases}$$

$$\begin{cases} \boldsymbol{P}_{p+1}^f = [\boldsymbol{I} - \boldsymbol{A}_{p+1}(p+1)\boldsymbol{B}_{p+1}(p+1)]\boldsymbol{P}_p^f \\ \boldsymbol{P}_{p+1}^b = [\boldsymbol{I} - \boldsymbol{B}_{p+1}(p+1)\boldsymbol{A}_{p+1}(p+1)]\boldsymbol{P}_p^b \end{cases}$$

for $k = 1,2,\cdots p-1$

$$\begin{cases} \boldsymbol{A}_{p+1}(k) = \boldsymbol{A}_p(k) + \boldsymbol{A}_{p+1}(p+1)\boldsymbol{B}_p(p+1-k) \\ \boldsymbol{B}_{p+1}(k) = \boldsymbol{B}_p(k) + \boldsymbol{B}_{p+1}(p+1)\boldsymbol{A}_p(p+1-k) \end{cases}$$

end for

for $n = p+1, p+2, \cdots N$

$$\begin{cases} \boldsymbol{e}_{p+1}^f[n] = \boldsymbol{e}_p^f[n] + \boldsymbol{A}_{p+1}(p+1)\boldsymbol{e}_p^b[n-1] \\ \boldsymbol{e}_{p+1}^b[n] = \boldsymbol{e}_p^b[n-1] + \boldsymbol{B}_{p+1}(p+1)\boldsymbol{e}_p^f[n] \end{cases}$$

end for

end while

are demonstrated in Figure 2(a) and Figure 3(a). The results show that they are coherent (MSC greater than 0.5) at the respiratory frequency. In addition, the response delay in PPG induced by respiration is also implied in the negative coherence phase (see Figure 2(a)). The respiration induced component is evident in the AR-based PSD of PPG signal, as shown in Figure 2(b). The coherence analysis is also specific to respiration. As the breath is in holding status, no coherent peak was found (see Figure 3). The coherent phenomenon cannot be observed by the FFT-based cross-spectrum method (as shown in Figure 4).

The existence of coherent peak is determined by whether the corresponding pole inside the unit circle is prominent or not. It has been shown that the coherence spectrum is sensitive and specific to the

respiration in this research, it may be possible to acquire the respiratory information from the PPG signal by single-channel AR method with the consideration of poles around the respiratory frequency. It may provide another attractive approach to acquire the respiratory information from PPG signal without the need of filtering. It also implies the possibility to acquire the other physiological parameters other than arterial oxygen saturation form pulse oximeters. Besides, the two-channel AR method introduced in section 2 can be easily expanded to more than three channels. Such multi-channel AR method may be an alternative attractive tool for the coherent analysis among respiration, central venous pressure (CVP), arterial blood pressure (ABP) and PPG signal in the related research, e.g. for the cases in intensive care unit (ICU) or during surgical operation.

ACKNOWLEDGEMENTS

The author wishes to express the gratitude to the National Science Council, Taiwan, for the financial support on this research (under contract number NSC 97-2221-E-035-001-MY3 and NSC 97-2221-E- 035-053).

REFERENCES

Hertzman, A. B. and Spielman, C. R., 1937, Observations on the finger volume pulse recorded photoelectrically. In *Am. J. Physiol.*, vol.119, pp.334-335.

Johansson, A., Öberg, P. Å. and Sedin, G., 1999, Monitoring of heart and respiratory rates in newborn infants using a new photoplethysmographic technique. In *J. Clin. Monit.*, vol.15, pp.461-467.

Johansson, A. and Öberg, P. Å., 1999a, Estimation of respiratory volumes from the photoplethysmographic signal. Part I: experimental results. In *Med. Biol. Eng. Comput.*, vol.37, pp.42-47.

Johansson, A. and Öberg, P. Å., 1999b, Estimation of respiratory volumes from the photoplethysmographic signal. Part II: a model study. In *Med. Biol. Eng. Comput.*, vol.37, pp.48-53.

Levinson, N., 1947, The Wiener RMS (root mean square) error criterion in filter design and prediction. In *J. Math. Phys.*, vol.25, pp.261-278.

Morf, M., Vieira, A., Lee, D. T. and Kailath, T., 1978, Recursive multichannel maximum entropy spectral estimation. In *IEEE Trans. Geosci. Electron.*, vol.16, pp.85-94.

Nilsson, L., Johansson, A. and Kalman, S., 2000, Monitoring of respiratory rate in postoperative care using a new photoplethysmographic technique. In *J. Clin. Monit.*, vol.16, pp.309-315.

Nilsson, L., Johansson, A. and Kalman, S., 2003, Macrocirculation is not the sole determinant of respiratory induced variations in the reflection mode photoplethysmographic signal. In *Physiol. Meas.*, vol.24, pp.925- 937.

Webster, J. G. Ed., 1997, *Design of Pulse Oximeters*, IOP Publishing, Bristol.

Welch, P. D., 1970, The use of the fast Fourier transform for the estimation of power spectra. In *IEEE Trans. Audio Electroacoust.*, vol.AU-15, pp.70-73.